Anal. Chem. **2008,** *80,* 6449–6457

Dual Fluorescence Sensor for Trace Oxygen and Temperature with Unmatched Range and Sensitivity

Carlos Baleizão,*,†,‡ Stefan Nagl,‡ Michael Schäferling,‡ Mário N. Berberan-Santos,† and Otto S. Wolfbeis‡

CQFM-Centro de Química-Física Molecular and IN-Institute of Nanoscience and Nanotechnology, Instituto Superior Técnico, Universidade Técnica de Lisboa, P-1049-001 Lisboa, Portugal, and Institute of Analytical Chemistry, Chemo- and Biosensors, University of Regensburg, 93040 Regensburg, Germany

An optical dual sensor for oxygen and temperature is presented that is highly oxygen sensitive and covers a broad temperature range. Dual sensing is based on luminescence lifetime measurements. The novel sensor contains two luminescent compounds incorporated into polymer films. The temperature-sensitive dye (ruthenium tris-1,10-phenanthroline) has a highly temperature-dependent luminescence and is incorporated in poly(acrylonitrile) to avoid cross-sensitivity to oxygen. Fullerene C_{70} was used as the oxygen-sensitive probe owing to its strong thermally activated delayed fluorescence at elevated temperatures that is extremely oxygen sensitive. The cross-sensitivity of C_{70} to temperature is accounted for by means of the temperature sensor. C_{70} is incorporated into a highly oxygen-permeable polymer, either ethyl cellulose or organosilica. The two luminescent probes have different emission spectra and decay times, and their emissions can be discriminated using both parameters. Spatially resolved sensing is achieved by means of fluorescence lifetime imaging. The response times of the sensor to oxygen are short. The dual sensor exhibits a temperature operation range between at least 0 and 120 °C, and detection limits for oxygen in the ppbv range, operating for oxygen concentrations up to at least 50 ppmv. These ranges outperform all dual oxygen and temperature sensors reported so far. The dual sensor presented in this study is especially appropriate for measurements under extreme conditions such as high temperatures and ultralow oxygen levels. This dual sensor is a key step forward in a number of scientifically or commercially important applications including food packaging, for monitoring of hyperthermophilic microorganisms, in space technology, and safety and security applications in terms of detection of oxygen leaks.

Oxygen, being essential for life, is an immensely important chemical species. Determination of oxygen levels is required in numerous areas, including medicine, biotechnology, aerospace research, food packaging, and the chemical industry. After the invention of the first optical, fluorescence-based sensor for oxygen 40 years ago,[1] it appeared hardly likely that optical sensors would rival the very successful and sensitive electrochemical oxygen measurement technique based on Clark electrodes. In the last decades, the potential offered by specific advantages of optical methods has been realized to a large extent. Among the many optical methods employed for sensing, fluorescence has attracted special attention because it is highly sensitive, versatile, noninvasive, and of low toxicity.[2,3] Fluorescence-based sensors, in not requiring a physical contact with the medium during measurement, are advantageous compared to contact sensors in applications where electromagnetic noise is strong or it is physically difficult to connect a wire. Further advantages of sensors based on molecular fluorescence are the very fast response, the reversibility, and the spatial resolution that can go from the macroscale (fluorescent paints) down to the nanoscale (fluorescence microscopy). These properties also overcome the limitations of electrochemical sensors, which are difficult to miniaturize, invasive, and limited to discrete points.[4]

All known fluorescence-based oxygen sensors, and in fact almost any sensor, no matter what type, suffer from interference by temperature. This interference can be corrected for using a second sensor to measure temperature. True multiple sensing methods are based on the use of a single sensor that yields a large amount of optical data, which provides information on more than one physical or chemical parameter.[5] Up to date, several kinds of dual sensors have been described, e.g., for CO_2/O_2,[6–8] O_2/T,[9–15] and pH/O_2.[16–18]

* To whom correspondence should be addressed. Tel.: +351 218-419-206. Fax: +351 218-464-455. E-mail: carlos.baleizao@ist.utl.pt.

† Universidade Técnica de Lisboa.

‡ University of Regensburg.

(1) Bergman, I. *Nature* **1968**, *218*, 396.
(2) *Optical Sensors for Industrial, Environmental and Clinical Applications*; Narayanaswamy, R., Wolfbeis O. S., Eds.; Springer: Berlin, 2004.
(3) Wolfbeis, O. S. *Anal. Chem.* **2008**, *80*, 4269−4283;. and previous biannual reviews.
(4) *Optical Chemical Sensors*; Baldini F., Chester, A. N., Homola, J., Martellucci, S., Eds; Springer: Dordrecht, 2006.
(5) Nagl, S.; Wolfbeis, O. S. *Analyst* **2007**, *132*, 507–511.
(6) Wolfbeis, O. S.; Weis, L. J.; Leiner, M. J. P.; Ziegler, W. E. *Anal. Chem.* **1988**, *60*, 2028–2030.
(7) Borisov, S. M.; Krause, C.; Arain, S.; Wolfbeis, O. S. *Adv. Mater.* **2006**, *18*, 1511–1516.
(8) Schroeder, C. R.; Neurauter, G.; Klimant, I. *Microchim. Acta* **2007**, *158*, 205–218.
(9) Coyle, L. M.; Gouterman, M. *Sens. Actuators, B* **1999**, *61*, 92–99.

10.1021/ac801034p CCC: $40.75
Published on Web 07/24/2008

Pressure-sensitive paints (PSPs) and temperature-sensitive paints have been the subject of intense research that contributed to vast progress in the past years.[19,20] PSPs are essentially oxygen sensors that take advantage of the fact that the fraction of oxygen in air is constant, allowing the calculation of total pressure from the oxygen partial pressure.[21] With these materials, it is possible to record the entire surface distribution of a large object (e.g., an aircraft in a wind tunnel), rather than just discrete points as with other sensors.[22] Sometimes, only trace concentrations of oxygen are employed in wind tunnels because sensor response is most sensitive under these conditions as a result of the Stern−Volmer equation.

Most of the food found in supermarkets is processed and stored in the absence of oxygen (modified atmosphere packaging).[23,24] At the same time, food requires a specific range of temperatures during storage and transport to maximize its shelf life. Dual oxygen and temperature fluorescence sensors also have found application in this area, especially because it is a remote and noninvasive method, meaning that oxygen and temperature can be monitored without any contact to the sealing.[25,26]

Oxygen and temperature sensing also play a crucial role in the area of microbiology, namely, in growth monitoring. Optical sensors are being increasingly used, and a number of fluorescent dual sensors have been described recently.[7,18] It is challenging in this field to monitor organisms that grow under unusual conditions, e.g., hyperthermophilic organisms that require high temperatures,[27] and atmospheres of residual oxygen to anaerobic conditions.[27] These organisms are also candidates for hydrogen production in a future hydrogen economy.[28] Another area of interest is chemical process and reaction monitoring. Many chemical reactions need to be carried out in the complete absence of oxygen and at high temperatures. Optical sensors enable us to observe the reaction parameters without disturbance, but at present, they are limited to moderate temperatures and not applicable at trace oxygen levels.[9–15]

A variety of devices and sensors based on molecular optical properties has been developed to measure oxygen partial pressure.[29,30] For trace oxygen sensing, the choice of sensors is between palladium and platinum porphyrins or ruthenium complexes that most often are immobilized in oxygen-permeable materials, with sensitivities in the ppmv range.[31,32] Another approach toward trace oxygen sensing is based on the thermally activated delayed fluorescence (TADF) effect displayed by C_{70}, leading to an extremely efficient quenching of the intensity and lifetime of TADF and, hence, resulting in sensitivities in the ppbv range.[33]

Temperature sensing based on luminescence lifetime changes, using fiber optics in combination with phosphors, is a well-established method.[34] More recently, several studies have been devoted to fluorescence-based molecular thermometry,[35,36] by exploiting the temperature dependence of either intensity, quantum yield, or lifetime of the luminescence of hydrocarbons, the exciplex formation in anilines and perylenes, of fluorescence quenching,[37] and of the TADF of fullerenes.[38–40]

Most dual sensors of O_2/T reported so far[9–15] have in common a single excitation wavelength in the visible region, luminescence decay time as the analytical signal, a single matrix to disperse both temperature and oxygen probes, and working ranges from 0 to 70 °C and over O_2 concentrations in the 0−100% range. Detection limits in the best cases, are at ppmv values. We describe here a dual sensor for simultaneous sensing of oxygen concentrations below 50 ppmv and temperatures up to 120 °C, based on luminescence lifetime measurements and that we assume to be useful in the areas outlined above.

EXPERIMENTAL SECTION

Materials. C_{70} (>99.9%), ruthenium(II)-tris-1,10-phenanthroline chloride hydrate, titanium dioxide, hexane, toluene, and ethyl cellulose 49 (EC) were purchased from Sigma-Aldrich (www.sigmaaldrich.com). Silicone RS 692-542 was obtained from RS Components (www.rs-components.com). Dimethylformamide (Acros, www.acros.com) was used as received. Polyacrylonitrile (PAN, powder, M_w ~170 000) was purchased from Polysciences (www.polysciences.com). Ruthenium(II)-tris-1,10-phenanthroline

(10) Hradil, J.; Davis, C.; Mongey, K.; McDonagh, C.; MacCraith, B. D. *Meas. Sci. Technol.* **2002**, *13*, 1552–1557.
(11) Zelelow, B.; Khalil, G. E.; Phelan, G.; Carlson, B.; Gouterman, M.; Callis, J. B.; Dalton, L. R. *Sens. Actuators, B* **2003**, *96*, 304–314.
(12) Köse, M. E.; Carroll, B. F.; Schanze, K. S. *Langmuir* **2005**, *21*, 9121–9129.
(13) Borisov, S. M.; Wolfbeis, O. S. *Anal. Chem.* **2006**, *78*, 5094–5101.
(14) Borisov, S. M.; Vasylevska, A. S.; Krause, C.; Wolfbeis, O. S. *Adv. Funct. Mater.* **2006**, *16*, 1536–1542.
(15) Stich, M. I. J.; Nagl, S.; Wolfbeis, O. S.; Henne, U.; Schaeferling, M. *Adv. Funct. Mater.* **2008**, *18*, 1399–1406.
(16) Vasylevska, G. S.; Borisov, S. M.; Krause, C.; Wolfbeis, O. S. *Chem. Mater.* **2006**, *18*, 4609–4616.
(17) Schröder, C. R.; Polerecky, L.; Klimant, I. *Anal. Chem.* **2007**, *79*, 60–70.
(18) Kocincová, A. S.; Nagl, S.; Arain, S.; Krause, C.; Borisov, S. M.; Arnold, M.; Wolfbeis, O. S. *Biotechnol. Bioeng.* **2008**, *100*, 430–438.
(19) *Pressure and Temperature Sensitive Paints*; Liu, T., Sullivan, J. P., Eds; Springer: New York, 2005.
(20) *Frontiers in Chemical Sensors*; Orellana, G., Moreno-Bondi, M. C., Eds; Springer: Berlin, 2005.
(21) Mitsuo, K.; Asai, K.; Takahashi, A.; Mizushima, H. *Meas. Sci. Technol.* **2006**, *17*, 1282–1291.
(22) Kontis, K. *Aeronautical J.* **2007**, *111*, 495–508.
(23) Mills, A. *Chem. Soc. Rev.* **2005**, *34*, 1003–1011.
(24) Valverde, J. M.; Guillen, F.; Martinez-Romero, D.; Castillo, S.; Serrano, M.; Valero, D. *J. Agric. Food Chem.* **2005**, *53*, 7458–7464.
(25) Fitzgerald, M.; Papkovsky, D. B.; Smiddy, M.; Kerry, J. P.; O'Sullivan, C. K.; Buckley, D. J.; Guilbault, G. G. *J. Food Sci.* **2001**, *66*, 105–110.
(26) Papkovsky, D. B.; Smiddy, M. A.; Papkovskaia, N. Y.; Kerry, J. P. *J. Food Sci* **2002**, *67*, 3164–3169.
(27) *Extremophiles*; Rainey, F. A., Oren, A., Eds; Academic Press: Amsterdam, 2006.
(28) de Vrije, T.; Mars, A. E.; Budde, M. A. W.; Lai, M. H.; Dijkema, C.; de Waard, P.; Claassen, P. A. M. *Appl. Microbiol. Biotechnol.* **2007**, *74*, 1358–1367.
(29) Ramamoorthy, R.; Dutta, P. K.; Akbar, S. A. *J. Mater. Sci.* **2003**, *38*, 4271–4282.
(30) DeGraff B. A.; Demas, J. N. In *Reviews in Fluorescence 2005*; Geddes C. D., Lakowicz, J. R., Eds; Springer Science: New York, 2005; pp 125−150.
(31) Apostolidis, A.; Klimant, I.; Andrzejewski, D.; Wolfbeis, O. S. *J. Comb. Chem.* **2004**, *6*, 325–331.
(32) Han, B. H.; Manners, I.; Winnik, M. A. *Chem. Mater.* **2005**, *17*, 3160–3171.
(33) Nagl, S.; Baleizão, C.; Borisov, S. M.; Schäferling, M.; Berberan-Santos, M. N.; Wolfbeis, O. S. *Angew. Chem., Int. Ed.* **2007**, *46*, 2117–2119.
(34) *Fiber Optic Fluorescence Thermometry*; Grattan, K. T., Zhang, Z. Y., Eds; Chapman and Hall: London, 1995.
(35) Demas, J. N.; DeGraff, B. A. *Coor. Chem Rev.* **2001**, *211*, 317–351.
(36) Uchiyama, S.; de Silva, A. P.; Iwau, K. *J. Chem. Educ.* **2006**, *83*, 720–727.
(37) Amao, Y. *Microchim. Acta* **2003**, *143*, 1–12.
(38) Berberan-Santos, M. N.; Garcia, J. M. M. *J. Am. Chem. Soc.* **1996**, *118*, 9391–9394.
(39) Baleizão, C.; Berberan-Santos, M. N. *J. Fluoresc.* **2006**, *16*, 215–219.
(40) Baleizão, C.; Nagl, S.; Borisov, S. M.; Schäferling, M.; Wolfbeis, O. S.; Berberan-Santos, M. N. *Chem. Eur. J.* **2007**, *13*, 3643–3651.

3-trimethylsilyl-1-propanesulfonate [Ru(phen)$_3$][41] and organosilica (OS)[42] were prepared according to the literature.

Methods. *Preparation of the Two-Layer Dual Sensors.* The sensor layers were prepared in two steps. First, a layer of Ru(phen)$_3$/PAN in dimethylformamide (DMF) was spread onto a polyester foil and after evaporation of the solvent, a second layer of C_{70}/OS or C_{70}/EC, both in toluene, was spread over the first layer. The Ru(phen)$_3$/PAN mixture was prepared by mixing Ru(phen)$_3$ (2 mg) and PAN (100 mg) in DMF (1.9 g) and stirring for 20 min at 50 °C. The mixture was spread as 120-μm-thick films (using a coater from RK Print-Coat Instruments Ltd.; www.rk-print.com) onto a 125 μm poly(ethylene terephthalate) (Mylar) foil from Goodfellow (www.goodfellow.com). The solvent was allowed to evaporate to yield a layer of ~6 μm thickness. The C_{70}/OS layer was prepared by dissolving C_{70} (1 mg) and OS (100 mg) in toluene (0.9 g) and stirring at room temperature for 15 min. C_{70}/EC was obtained by dissolving C_{70} (1 mg) and EC (100 mg) in toluene (1.9 g), and the solution was ultrasonicated and heated at 40 °C for 15 min. Both solutions were spread as 120-μm-thick films over the Ru(phen)$_3$/PAN layer to yield dry layers of ~12 (C_{70}/OS) and 6 μm (C_{70}/EC) thicknesses. The reflective layer was prepared by dissolving 1 g of one-component silicone RS692-542 and 0.3 g of TiO_2 in 0.7 g of hexane, and after 30 min of stirring, it was knife-coated as 120-μm-thick films onto the 125 μm polyester foil and left for curing overnight.

Spectral Characterization. Absorption and emission spectra were recorded on a Lambda 14 P UV−vis spectrophotometer (www.perkinelmer.com) and Aminco AB 2 luminescence spectrometer (www.thermo.com), respectively.

Sensor Calibration. All measurements were carried out in a self-developed custom flow chamber, where a piece of the sensor strip was placed along with the scatter layer. The chamber was connected to a RC6 thermostat from Lauda (www.lauda.com) which ran on silicon oil M 10 from Roth (www.roth.de). The gas flow in the cell was adjusted by two PR 4000 pressure controllers (MKS Instruments, www.mksinst.com). Calibration gases (nitrogen and 50 ppm O_2 in nitrogen) were obtained from Linde (www.linde-gase.de).

Imaging of C_{70} and Ru(phen)$_3$. The optical setup was identical to that in earlier studies.[33,40] Excitation light was filtered through an FITCA filter (Schott, www.schott.de). Emission was recorded through a Chroma 680 filter for the fullerene and a Chroma 580 filter for the Ru complex, both filters having a full width at half-maximum of ~60 nm (AHF Analysentechnik, www.ahf.de). For calculation of luminescence lifetimes, the rapid lifetime determination (RLD) method was used.[43] Following a square-shaped light pulse, luminescence was detected quantitatively in two different gates. The first gate (G_1) was only opened after a delay period after switching off the LEDs. This suppresses short-lived background fluorescence almost quantitatively. Potential interferences caused by backscattered excitation light are also eliminated in this manner. The second gate (G_2) is opened immediately after the closure of G_1. In the case of Ru(phen)$_3$, the gates started 250 and 1250 ns after switching off the LEDs, they were 1 μs long each, and the LED was turned on for 4 μs with a repetition rate of 100 kHz. For C_{70}, the gates started 100 and 5100 μs after switching off the LEDs, they were 5 ms long each, and the LED was turned on for 30 ms with a repetition rate of 10 Hz. The ratio G_1/G_2 is virtually independent of the overall signal intensity. Assuming a constant aperture time for each gate, the average decay time τ of each pixel can be calculated as $\tau = \Delta t/\ln(G_1/G_2)$where Δt is the integration time and G_1 and G_2 are the areas of each gate.

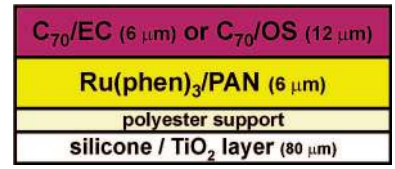

Figure 1. Cross section of the sensor layers for simultaneous optical sensing and imaging of oxygen and temperature. The luminescence of the compounds is excited from above, and emission is also collected there. The TiO_2 reflective layer acts as a scattering area to increase the intensity of the luminescence collected above.

RESULTS AND DISCUSSION

Composition, Calibration, and Properties of the Dual Sensors. The material contains two sensor layers, each with the luminescent probe dispersed in a polymer matrix, thus allowing simultaneous determination of oxygen partial pressure and temperature. Figure 1 schematically shows the cross section of the final composite sensor material.

The accurate sensing of oxygen and temperature is often affected by the mutual cross-sensitivities of the indicators, which have to be minimized. The cross-sensitivities can result from several effects: (i) overlap of the luminescence signals from both probes; (ii) temperature dependence of the lifetime and quenching kinetics of the oxygen probe; or (iii) quenching of the temperature probe by oxygen. To avoid the cross-sensitivities and to achieve optimal sensitivities, both probes and polymers must be carefully chosen.

The luminescences of ruthenium(II) polypyridyl complexes exhibit a strong temperature dependence.[35] In particular, ruthenium(II) tris(phenanthroline) (Ru(phen)$_3$) is a common optical temperature probe that displays efficient temperature quenching and therefore high sensitivity.[41] Ru(phen)$_3$ complexes can be easily incorporated into solid matrixes, such as sol−gels or polymers.[4,44,45] The photostability of these complexes is rather high in the absence of oxygen, and they can be excited in the visible region. The brightness (defined as the product of the molar absorption coefficient ϵ and the quantum yield Φ) of Ru(phen)$_3$ in PAN at room temperature is ~2000 and decreases to 200 at 100 °C.[40,46] The luminescence of Ru(II) polypyridyl complexes is quenched by oxygen. In order to avoid this interference when sensing temperature, the Ru(phen)$_3$ complex was immobilized in PAN. The extremely low gas permeability of PAN ($P = 1.5 \times 10^{-17}$ cm^2 Pa s^{-1})[47] in essence eliminates quenching by oxygen.

(41) Liebsch, G.; Klimant, I.; Wolfbeis, O. S. *Adv. Mater.* **1999**, *11*, 1296–1299.
(42) Brusatin, G.; Innocenzi, P. *J. Sol-Gel Sci. Technol.* **2001**, *22*, 189–204.
(43) Liebsch, G.; Klimant, I.; Frank, B.; Holst, G.; Wolfbeis, O. S. *Appl. Spectrosc.* **2000**, *54*, 548–559.
(44) Wolfbeis, O. S. *J. Mater. Chem.* **2006**, *15*, 2657–2669.
(45) *Fluorescence of Supermolecules, Polymers, and Nanosystems*; Berberan-Santos, M. N., Ed.; Springer: Berlin, 2008.
(46) Alford, P. C.; Cook, M. J.; Lewis, A. P.; McAuliffe, S. G.; Skarda, V.; Thomson, A. J. *J. Chem. Soc., Perkin Trans. 2* **1985**, *5*, 705–709.
(47) Brandrup, J., Immergut, E. H. Grulke, E. A. *Polymer Handbook*; Wiley: New York, 1999.

Fullerene C_{70} displays the TADF effect. In fact, there are two distinct unimolecular mechanisms for its fluorescence: prompt fluorescence (PF) and TADF.[48,49] In the PF mechanism, emission occurs after $S_n \leftarrow S_0$ absorption and excited-state relaxation to S_1. The TADF mechanism takes place via the triplet manifold: after excitation to the S_1 state, intersystem crossing (ISC) to the triplet manifold (T_1 or a higher triplet) occurs, followed by a second ISC from T_1 back to S_1, and by prompt fluorescence. The cycle $S_1 \rightarrow T_1 \rightarrow S_1$ may be repeated a number of times before fluorescence finally takes place.[50] TADF is significant only when several conditions are met: a small energy gap between S_1 and T_1 (ΔE_{ST}), a long T_1 lifetime, and temperature high enough for this process to take place.[38] For most fluorophores, TADF is usually much weaker than PF. Although known for many years, TADF continues to be a rare phenomenon, with a few observations in some xanthene dyes,[49,51,52] aromatic ketones[53,54] and thiones,[55,56] metal porphyrins,[57] imidazole derivatives,[58] and aromatic hydrocarbons.[59,60]

The photophysical properties of fullerene C_{70} are remarkable in that the Φ_T is close to 1,[61] the ΔE_{ST} gap[62] is small, and the intrinsic phosphorescence lifetime is rather long.[63] Such properties are required for the exceptionally strong TADF[35] found to occur. C_{60}[64] and some C_{60} derivatives,[65,66] as well as one C_{70} derivative,[67] also exhibit TADF, but with much less efficiency than C_{70}.

The outstanding TADF effect displayed by C_{70} with a maximal increase in the quantum yield by a factor of ~100, and the fact that TADF lifetimes fall in the millisecond range,[40] are most useful features for the development of a trace oxygen sensor. Its sensitivity to O_2 increases with T because the molecule resides longer in the triplet state (and more efficiently interacts with (triplet) oxygen) at higher temperatures. On the other hand only the unique TADF effect, based on a cycling of the molecule between singlet and a triplet excited states ensures that the molecule still has a quantum yield high enough to be practically useful. This effect is uniquely strong in C_{70}. The oxygen probe was dissolved in EC or OS, which are among the most permeable materials toward oxygen.[47] The value of brightness for C_{70} (less than 10 at room temperature) is 2 orders of magnitude lower than that of the Ru(phen)$_3$ complex. However, upon oxygen removal, the quantum yield increases by 20 times at room temperature and 80 times at 100 °C, and the brightness reaches values similar or even higher to those of the ruthenium complex.[40]

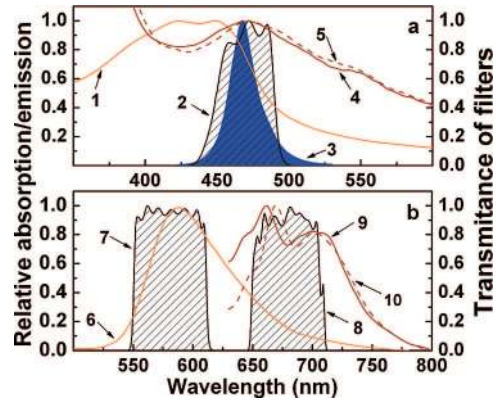

Figure 2. Spectra of the materials and components used in the dual sensor system: (1) absorption of Ru(phen)$_3$ in PAN; (2) transmittance of the interference filter FITCA; (3) emission of the light source (LED 470); (4, 5) absorption of C_{70} (in EC and OS, respectively); (6) fluorescence of Ru(phen)$_3$ in PAN; (7, 8) transmittance of the emission interference filters (Chroma 580 and Chroma 680, respectively); (9, 10) fluorescence of C_{70} (in EC and OS, respectively).

Excitation and emission of the luminescent compounds are detected from the top. To increase the collection of exciting and emitted light (backscatter luminescence), a reflective layer of TiO−silicone rubber composition was placed at the backside of the sensor layer. The absorption and emission of the luminescent compounds, the spectral data of the filters, and the spectrum of the light source (LED) are shown in Figure 2.

The Ru(phen)$_3$ complex and C_{70} in the polymer support exhibit similar absorption maximums in the visible. This is an advantage for the instrumental setup, as only a single excitation source is required to excite both probes. The excitation source used was a blue LED (with a 470 nm peak wavelength) whose light passes a 488 nm interference filter (Schott FITCA). The emission spectra of the two compounds are quite different. While Ru(phen)$_3$ has an emission maximum around 580 nm, C_{70} shows its maximum in the region from 670 to 700 nm. The luminescence signals are separated by appropriate emission filters, and the red part of the Ru(phen)$_3$ emission, which partially overlaps the emission window of C_{70}, was suppressed in the time domain.

The two-layer material described here has the advantage of suppressing any resonance energy transfer from Ru(phen)$_3$ to C_{70} as a result of their spatial separation.

The calibration of the sensor was performed by time-domain fluorescence lifetime imaging, with the determination of the lifetime of the indicators at several oxygen concentrations and temperatures, using the RLD method.[43] The use of decay time is advantageous when compared to intensity-based methods in that interferences from drifts of the sensor and the optoelectonic system are minimized because lifetime is independent of the local

(48) Valeur, B. *Molecular Fluorescence: Principles and Applications*; Wiley: Weinheim, 2002.
(49) Parker, C. A. *Photoluminescence of Solutions*; Elsevier: Amsterdam, 1968.
(50) Baleizão, C.; Berberan-Santos, M. N. *J. Chem. Phys.* **2007**, *126*, 204510.
(51) Lam, S. K.; Lo, D. *Chem. Phys. Lett.* **1997**, *281*, 35–43.
(52) Duchowicz, R.; Ferrer, M. L.; Acuña, A. U. *Photochem. Photobiol.* **1998**, *68*, 494–501.
(53) Wolf, M. W.; Legg, K. D.; Brown, R. E.; Singer, L. A.; Parks, J. H. *J. Am. Chem. Soc.* **1975**, *97*, 4490–4497.
(54) Turek, A. M.; Krishnammorthy, G.; Phipps, K.; Saltiel, J. *J. Phys. Chem. A* **2002**, *106*, 6044–6052.
(55) Maciejewski, A.; Szymanski, M.; Steer, R. P. *J. Phys. Chem.* **1986**, *90*, 6314–6318.
(56) Eisenberger, H.; Nickel, B. *J. Chem. Soc., Faraday Trans.* **1996**, *92*, 733–740.
(57) Yusa, S.; Kamachi, M.; Morishima, Y. *Photochem. Photobiol.* **1998**, *67*, 519–525.
(58) Park, S.; Kwon, O. H.; Lee, Y. S.; Jang, D. J.; Park, S. Y. *J. Phys. Chem. A* **2007**, *111*, 9649–9653.
(59) Nickel, B.; Klemp, D. *Chem. Phys.* **1993**, *174*, 297–318.
(60) Nickel, B.; Klemp, D. *Chem. Phys.* **1993**, *174*, 319–330.
(61) Arbogast, J. W.; Foote, C. S. *J. Am. Chem. Soc.* **1991**, *113*, 8886–8889.
(62) Argentine, S. M.; Kotz, K. T.; Francis, A. H. *J. Am. Chem. Soc.* **1995**, *117*, 11762–11767.
(63) Wasielewski, M. R.; O'Neil, M. P.; Lykke, K. R.; Pellin, M. J.; Gruen, D. M. *J. Am. Chem. Soc.* **1991**, *113*, 2774–2776.
(64) Salazar, F. A.; Fedorov, A.; Berberan-Santos, M. N. *Chem. Phys. Lett.* **1997**, *271*, 361–366.
(65) Gigante, B.; Santos, C.; Fonseca, T.; Curto, M. J. M.; Luftmann, H.; Bergander, K.; Berberan-Santos, M. N. *Tetrahedron* **1999**, *55*, 6175–6182.
(66) Anthony, S. M.; Bachilo, S. M.; Weisman, R. B. *J. Phys. Chem. A* **2003**, *107*, 10674–10679.
(67) Bachilo, S. M.; Benedetto, A. F.; Weisman, R. B.; Nossal, J. R.; Billups, W. E. *J. Phys. Chem. A* **2000**, *104*, 11265–11269.

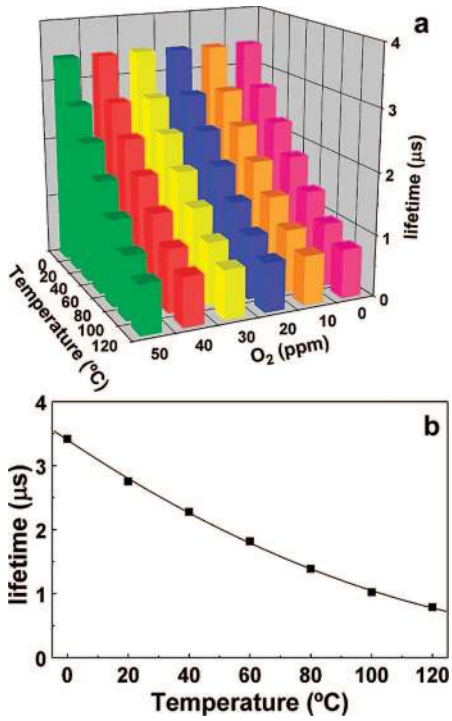

Figure 3. Ru(phen)$_3$/PAN-C_{70}/EC dual sensor: (a) calibration plot for the temperature system Ru(phen)$_3$/PAN and (b) temperature dependence of the average lifetimes of Ru(phen)$_3$/PAN shown as black squares with the solid line corresponding to the nonlinear fit to the data ($\tau = 8.2 \times 10^{-5}T^2 - 0.0318T + 3.4005$ with $r^2 = 0.999$). Oxygen concentrations are from 0 to 50 ppmv in nitrogen at atmospheric pressure.

dye concentration, turbidity of the sample, and scattering effects. The signal change caused by photobleaching is also usually much less significant when measuring lifetime rather than intensity. The RLD decay time sensing method is highly compatible with our system in enabling the separation of the fluorescence signals of Ru(phen)$_3$ and C_{70} with relatively simple instrumentation.

The lifetimes of both layers were determined at different oxygen concentrations (0−50 ppmv in nitrogen at atmospheric pressure) and temperatures (0−120 °C). The calibration plots for the temperature-sensitive system (Ru(phen)$_3$/PAN) in the dual sensor are presented in Figure 3. The decay times are unaffected by increasing oxygen concentration (Figure 3a). In fact, when changing the oxygen concentration between 0 and 50 ppmv, all measured lifetimes are within 0.31% deviation for all temperatures measured. The PAN film shields oxygen and prevents quenching, and therefore, the cross-sensitivity of the temperature indicator to oxygen is absent in our case.

The decay time of Ru(phen)$_3$ in PAN is highly temperature dependent by decreasing with increasing temperature, as can be seen from Figure 3b. This dependence is attributed to a thermally activated nonradiative decay channel.[35] The temperature dependence of the lifetime is well described by the following empirical equation (Figure 3b)

$$\tau = 8.2 \times 10^{-5}T^2 - 0.0318T + 3.4005 \qquad (1)$$

with τ in μs and T in °C. For each temperature, the standard deviation of the average lifetime of the Ru(phen)$_3$/PAN system at several oxygen concentrations is lower than 9 ns. The lifetime of the Ru(phen)$_3$/PAN system is independent of oxygen concentration, so that one can use the measured lifetime to determine the temperature at any fraction (or partial pressure) of oxygen, as described below.

The RLD method was used to image the temperature dependence of the Ru(phen)$_3$/PAN system, allowing us to determine the temperature at any point on the sensor's surface. Figure 4a shows the temperature dependence of the Ru(phen)$_3$ lifetime at different oxygen concentrations in pseudocolor code. The results allow the construction of the calibration plot shown in Figure 3a. The image profile displayed by the Ru(phen)$_3$/PAN layer is rather homogeneous at all temperatures.

The calibration plot for the oxygen-sensitive system (C_{70}/EC) in the dual sensor material was achieved by determining the lifetimes at different oxygen concentrations (0−50 ppmv in nitrogen at atmospheric pressure) and temperatures (0−120 °C) and is presented in Figure 5a. The lifetimes are highly temperature and oxygen dependent, as can be seen. In the absence of oxygen, fluorescence lifetime (τ_0) is 25.1 ms at 0 °C and drops to 8.0 ms at 120 °C. These lifetime decreases lead to a reduction of the sensitivity toward oxygen at elevated temperatures (Figure 5b), because the oxygen has less time to interact with C_{70}. However, the lifetime is still much higher than those of common probes (which show the same effect, just on faster time scales). The sensitivity to oxygen is still very high at 120 °C and most likely at even higher temperatures. This effect is also compensated for, to some extent, by the higher collisional rate with oxygen at higher temperatures.[33]

The quenching by oxygen is highly efficient for all temperatures, with the lifetime of C_{70} decreasing by 50−60% when the concentration of O_2 increases from 0 to 50 ppmv. As an example, the lifetime of C_{70} at 0 °C decreases from 25.1 to 10.0 ms, and at 120 °C from 8.0 to 4.1 ms. The Stern−Volmer plot ($(\tau_0/\tau) - 1$ versus $[O_2]$) for quenching of C_{70} is presented in Figure 5b. The "two-site model" was used to fit the data.[68] It is an extension of the standard Stern−Volmer model and formally assigns the sensor molecules to two different microenvironments within the polymer, with dissimilar oxygen permeability. It is a very viable method to account for the nonideal quenching found in many systems. Therefore, the quenching constants are different for these regions. The two-site model Stern−Volmer equation in the lifetime form reads

$$\frac{I}{I_0} = \frac{\tau}{\tau_0} = \frac{f_1}{1 + K_{SV}^1[O_2]} + \frac{f_2}{1 + K_{SV}^2[O_2]} \qquad (2)$$

where K_{SV}^1 and K_{SV}^2 are the Stern−Volmer constants for each component and f_1 and f_2 are the fractions of the total emission for each component, respectively (with $f_1 + f_2 = 1$).

The two-site model fits the experimental data very well (Figure 5b), in that r^2 in all cases is better than 0.998. Table 1 compiles the Stern−Volmer constants extracted from the fitting along with the detection limits. These are a function of temperature. The C_{70}/EC system exhibits an almost ideal ("one-site") behavior, with f_1 practically equal to unity (except for 0 °C), meaning that EC is highly homogeneous with respect to oxygen diffusion.

(68) Demas, J. N.; DeGraff, B. A. *Anal. Chem.* **1995**, *67*, 1377–1380.

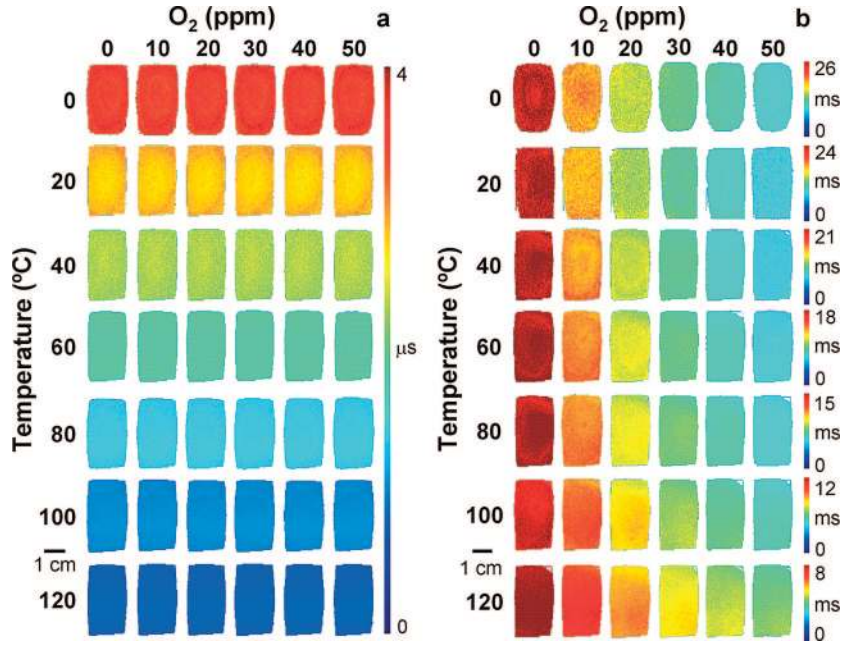

Figure 4. Pseudocolored fluorescence lifetime images of Ru(phen)$_3$/PAN (a) and C_{70}/EC (b) in the double sensor Ru(phen)$_3$/PAN−C_{70}/EC, between 0 and 120 °C and oxygen concentrations from 0 to 50 ppmv in nitrogen at atmospheric pressure.

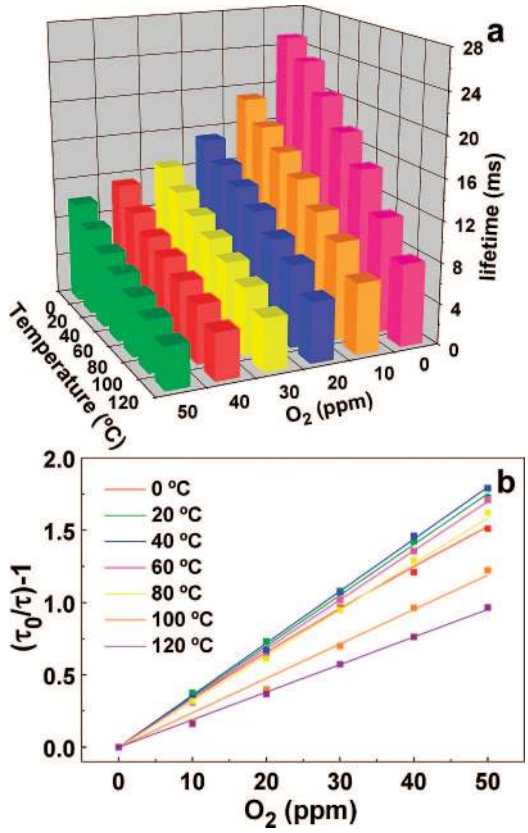

Figure 5. Ru(phen)$_3$/PAN−C_{70}/EC dual sensor: (a) calibration plot for the oxygen sensor C_{70}/EC; and (b) lifetime-based Stern−Volmer plots at various temperatures for the oxygen sensor C_{70}/EC. Oxygen concentrations from 0 to 50 ppmv in nitrogen at atmospheric pressure.

The limits of detection (LODs) are defined as the levels at which 1% quenching occurs. The C_{70}/EC system displays LODs in the ppbv range (between 280 and 530 ppbv). As far as we know, this is one of the lowest LODs reported for gas-phase oxygen sensors.[5]

Lifetime pseudocolor images of the oxygen-sensitive probe in the dual sensor are shown in Figure 4b. The oxygen dependence of the C_{70} lifetime results in the calibration plot in Figure 5. The image profile displayed by the C_{70}/EC layer also is rather homogeneous.

A second dual sensor material was evaluated for simultaneous sensing of oxygen and temperature. In this material, OS was used as the polymer for the oxygen system. The Ru(phen)$_3$/PAN−C_{70}/OS material was calibrated for temperatures between 0 and 120 °C and oxygen concentrations from 0 to 50 ppmv in nitrogen at atmospheric pressure (Figure S-1 and S-2, Supporting Information).[69] The temperature sensor is the same as the previous dual sensor material and displays identical behavior. The oxygen sensor is almost equally sensitive toward oxygen, with LODs in the ppbv range (see Table 1). Lifetime images of both systems were also recorded (Figure S-3, Supporting Information).[69] The C_{70}/OS system exhibit a high homogeneity over the entire range of conditions studied, favored by the high thermal stability of the silicone-based materials.

The response times to oxygen for both dual sensors were evaluated (Figure 6). The plots are based on time-resolved fluorescence intensity, because of the possibility of faster data acquisition when using only a single gate instead of two for the lifetime data. With our experimental setup, we could acquire data each 2 s. The time-resolved fluorescence intensity drops by more than 50% on both systems (OS 50% and EC 60%) when going from pure nitrogen to 50 ppmv oxygen in nitrogen (Figure 6). The time for 95% of the total signal change to occur (t_{95}) is less than 2 s for the transition from pure nitrogen to 50 ppmv in both polymers and most likely is limited by the time it takes for the gas to migrate from the mixing device to the flow chamber. The response can be regarded as practically instantaneous as would be expected

(69) See Supporting Information for more details.

Table 1. Stern−Volmer Constants and Detection Limits for Oxygen Sensing Using Fullerene C_{70} in Ethylcellulose or Organosilica at Various Temperatures

	C_{70}/EC		C_{70}/OS	
temperature (°C)	K_{SV}^{1}[a] (mg (O_2) $L^{-1})^{-1}$	detection limit[b,c] (μg (O_2) L^{-1})	K_{SV}^{1}[a] (mg (O_2) $L^{-1})^{-1}$	detection limit[b,c] (μg (O_2) L^{-1})
0	29.9 (0.93)	0.36 (0.29)	33.0 (0.88)	0.34 (0.27)
20	28.3 (1)	0.36 (0.29)	28.1 (0.94)	0.38 (0.31)
40	29.0 (1)	0.35 (0.28)	29.4 (0.95)	0.36 (0.29)
60	27.4 (1)	0.37 (0.28)	26.4 (0.99)	0.40 (0.33)
80	25.6 (1)	0.39 (0.32)	26.9 (0.93)	0.42 (0.34)
100	19.2 (1)	0.53 (0.42)	19.5 (1)	0.52 (0.42)
120	15.4 (1)	0.66 (0.53)	14.8 (1)	0.68 (0.55)

[a] In parentheses, f_1 from the "two-site" quenching model. [b] At 1% quenching ($\tau/\tau_0 = 0.99$). [c] In parentheses, the detection limits in ppmv of O_2. One microgram of O_2 per liter corresponds to a concentration of 31.25 nmol L^{-1} or 807 ppbv at atmospheric pressure.

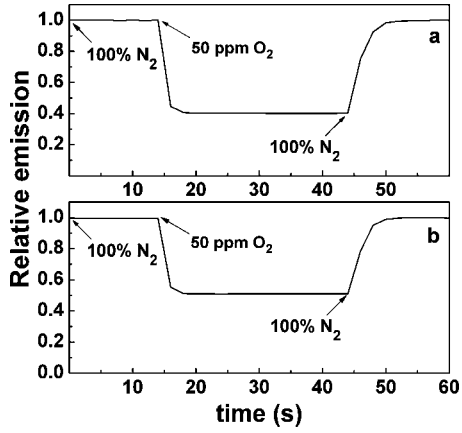

Figure 6. Fluorescence intensity response time plots for (a) C_{70}/EC and (b) C_{70}/OS at 20 °C and for oxygen concentrations between 0 and 50 ppmv in nitrogen at atmospheric pressure.

for these highly permeable polymers. The response in the reverse direction is somewhat slower, as it takes more time for the nitrogen to replace all the oxygen left in the polymer and is ~6 s (t_{95}) for both polymers.

The materials exhibit full reversibility, and the response time for oxygen variation in the low ppmv domain is extremely fast. The response of the materials is fully reversible many hundred times. The photostability is also high, no change in the fluorescence lifetimes being observed after several hours of continuous irradiation.

Derivation and Validation of a Bivariate Calibration Function for All Temperatures and Oxygen Concentrations Covered. Here, we aimed to construct a relatively simple semiempirical calibration function that allows calculating the oxygen concentration at any temperature within the calibration range, rather than just the temperatures, where the calibration was performed. The temperature dependence, thermal stability and photostability, response times, and sensitivity toward oxygen are very similar for both materials presented previously. However, the $Ru(phen)_3$/PAN−C_{70}/EC dual sensor material was selected because of its almost linear (one-site behavior) Stern−Volmer fits (see Table 1). Thus, we use only one Stern−Volmer constant in the subsequent calculations.

The Stern−Volmer equation with one constant reads

$$\frac{\tau_0}{\tau(T)} = 1 + K_{SV}[O_2] = 1 + k_q(T)\tau_0(T)[O_2] \qquad (3)$$

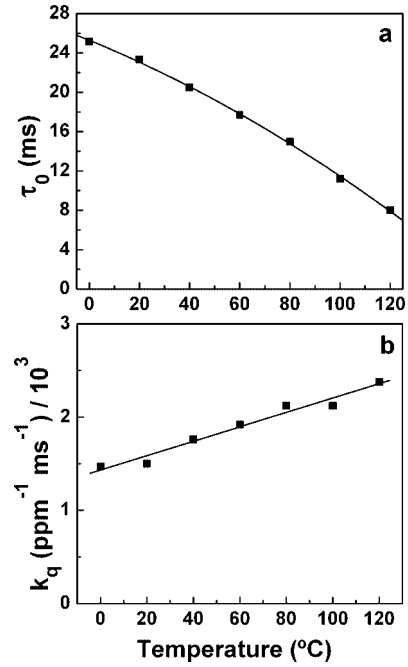

Figure 7. Temperature dependence plots of (a) τ_0 and (b) k_q for C_{70}/EC shown as black squares, with the solid lines corresponding to the nonlinear ($\tau_0 = -3.38 \times 10^{-4}T^2 - 0.104T + 25.28$ with $r^2 = 0.99$) and linear ($k_q = 7.71 \times 10^{-6}T + 1.43 \times 10^{-3}$ with $r^2 = 0.97$) fit to the data, respectively.

where the τ_0 is the lifetime in the absence of oxygen, τ is the lifetime in the presence of a predetermined concentration of oxygen, and k_q is the quenching constant. It can be rearranged to give

$$[O_2] = \frac{\dfrac{1}{\tau(T)} - \dfrac{1}{\tau_0(T)}}{k_q(T)} \qquad (4)$$

and hence to compute the oxygen concentration. However, it is first necessary to determine τ_0 and k_q, which are temperature dependent. Figure 7 shows the temperature dependence of τ_0 and k_q, and the nonlinear and linear fits to the data, respectively.

By inserting the fits given in Figure 7 into eq 4, we obtain

$$[O_2] = \frac{\dfrac{1}{\tau(T)} - \dfrac{1}{25.3 - 0.0104T - 3.38\times10^{-4}T^2}}{1.43\times10^{-3} + 7.71\times10^{-6}T} \qquad (5)$$

Table 2. Experimental Values from the Ru(phen)$_3$/PAN-C_{70}/EC Dual Sensor Calibration Function

experimental settings		calculated values	
T (°C)	O_2 (ppm)[a]	T (°C)[b]	O_2 (ppm)[c]
28.0	7.0	28.0 ± 0.4	7.2 ± 0.2
37.0	0.5	36.5 ± 0.4	0.7 ± 0.5
73.0	23.0	73.1 ± 0.1	22.3 ± 1.4

[a] O_2 concentrations in nitrogen at atmospheric pressure. [b] Calculated using eq 1. [c] Calculated using eq 5.

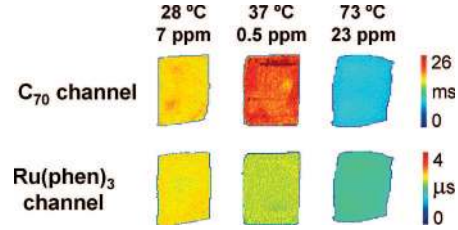

Figure 8. Pseudocolored fluorescence lifetime images of the dual sensor Ru(phen)$_3$/PAN−C_{70}/EC, using the experimental points from Table 2.

where T is the temperature (in °C). The temperature is determined from the lifetime of Ru(phen)$_3$/PAN using eq 1, and $\tau(T)$ is the lifetime of the oxygen probe (C_{70}/EC) measured at that same temperature.

The calibration functions were made using a set of experimental points with different temperatures and oxygen concentrations. The calculated values were determined using eq 1 for temperature and subsequently used in eq 5 as input for computing the oxygen concentration. Table 2 summarizes the experimental settings and the calculated values. In order to check the reproducibility of the system, several measurements were made for each set of points.

The calculated values are in good agreement with the experimental ones. Lifetime images were recorded for both systems and are presented in Figure 8. The images are in agreement with the results obtained from the calibration (see Figures 3 and 5). For even higher accuracy, the calibration can of course be extended including more temperatures, and the calibration function for oxygen can be extended to account for the deviations from linearity in the oxygen sensor. However, we have shown that it is possible to obtain relatively accurate results using the procedure described above (Table 2).

A comparison between fluorescence-based oxygen−temperature dual sensors reported so far and ours is presented in Table 3. The majority of the materials have common characteristics like a single excitation wavelength, luminescence decay time as the analytical information, an excitation wavelength in the visible region, and a single polymer matrix to disperse both sensors.

The materials reported so far use a single polymer to disperse both temperature and oxygen systems, while our materials use two polymers, one for each system. This is a disadvantage for large coatings, as the spreading procedure must be done twice. However, this strategy has the advantage to physically separate the two probes and therefore to avoid interferences such as energy transfer between the individual probes. It also allows choosing an optimal environment for each probe, rather than having to compromise in order to account for the requirements of both probes. The main advantages of our dual sensor are the operating temperature and oxygen concentration range. The materials reported so far display operation temperatures between 0 and 70 °C and 0−20 or 0−100% for oxygen concentrations, while our sensor is specifically suited for the determination of trace amounts of oxygen and covers a very wide temperature range. All other optical dual sensors with oxygen-sensing capabilities display less sensitivity and cannot be operated at such high temperatures because of their operating mechanism, which is mostly based on phosphorescence quenching. The Ru(phen)$_3$/PAN−C_{70}/EC and Ru(phen)$_3$/PAN−C_{70}/OS sensing materials cover a higher range of temperatures (between 0 and 120 °C) and allow the measurement of oxygen concentrations between 0 and 50 ppmv with LODs in the ppbv range (see Table 1). These sensors are also interesting with respect to the development of triple sensors, which is a topic of current research, aiming at the incorporation of probes sensitive to pH or CO_2 into T/O_2 dual sensors.

CONCLUSIONS

A dual sensor is presented for simultaneous sensing of temperature and oxygen, operating over a range of more than 100 °C, and specifically suited for detection of trace oxygen. The sensor takes advantage of the high temperature dependence of a Ru-polypyridyl complex and of the strong thermally activated delayed fluorescence exhibited by fullerene C_{70} and its high sensitivity toward O_2. The materials are photostable and display high storage stability. The oxygen sensor exhibits sensitivities in the ppbv range, one of the highest ever reported. The response

Table 3. Comparison between the Materials Used So Far for Dual Sensing of Temperature and Oxygen

temperature probe	oxygen probe	polymer	λ_{exc} (nm)[a]	signal[b]	T range (°C)	O_2 range (%)	ref
La_2O_2S:Eu_3 phosphor	Pt-TFPP	FIB	337	DT, TD	0−50	0−20	9
magnesium fluoro-germanate	Ru-dpp	sol−gel	470	DT, TD	25−65	0−100	10
Eu-β-diketonate complex	Pt-TFPP lactone	FIB	390	DT, I, TD	5−45	0−20	11
Ru-phen in PAN microbeads	Pt-TFPP	p-*t*BS-co-TFEM	465	I	10−50	0−20	12
Eu complexes in PTBS or PVMK microbeads	Pd-TFPP in PSAN microbeads	hydrogel for both particles	405	DT, FD	1−70	0−20	13
Ru-phen in PAN microbeads	Pd-TFPP in PSAN microbeads	hydrogel for both particles	470 (Ru) 525 (Pd)	DT, FD	1−60	0−100	14
Eu(tta)$_3$dpbt in PVC microbeads	Pt-TFPP in PSAN microbeads	hydrogel for both particles	405	DT, TD	1−50	1−40	15
Ru-phen in PAN film	C_{70} in OS or EC film		470	DT, TD	0−120	0−0.005 (0 - 50 ppmv)	this work

[a] For both luminophores, except when mentioned otherwise. [b] Analytical signal: DT, luminescence decay time; *I*, luminescence intensity; TD, time domain; FD, frequency domain.

time of the oxygen sensor within the concentration range used is less than a few seconds. A bivariate calibration function for the dual sensor was developed and validated, using a model that takes into account the effect of temperature on the oxygen sensor. The materials may find applications in areas as diverse as anaerobic (micro)biotechnological procedures, aerospace research, factory security, and the food packaging industry.

ACKNOWLEDGMENT

This work was partially supported by the German Center for Aerospace Research (DLR), by the Fundação para a Ciência e a Tecnologia (FCT, Portugal) and POCI 2010 (FEDER) within project POCI/QUI/58515/2004 C.B. was supported by a postdoctoral fellowship from Fundação para a Ciência e a Tecnologia, Portugal (SFRH/BPD/28438/2006).

SUPPORTING INFORMATION AVAILABLE

Additional information as noted in text. This material is available free of charge via the Internet at http://pubs.acs.org.

Received for review May 21, 2008. Accepted June 17, 2008.

AC801034P